Sonderdruck aus

ABHANDLUNGEN
DER AKADEMIE DER WISSENSCHAFTEN IN GÖTTINGEN

Mathematisch-Physikalische Klasse · Dritte Folge · Nr. 38

49

Small Scale Magnetic Flux Concentrations in the Solar Photosphere

Proceedings of a Workshop
held in Göttingen, 1–3 October 1985

Edited by
W. Deinzer, M. Knölker and H. H. Voigt

VANDENHOECK & RUPRECHT IN GÖTTINGEN
1986

Fully Dynamic Calculations of (Magneto-) Hydrodynamic Wave Propagation in Stellar Atmospheres

PETER ULMSCHNEIDER and DAVID MUCHMORE

Institut für theoretische Astrophysik
Im Neuenheimer Feld 561
6900 Heidelberg, Federal Republic of Germany

Abstract We review calculations of time-dependent (magneto-) hydrodynamic wave propagation in stellar atmospheres in which the fully dynamic coupling between the (magneto-) hydrodynamics, the thermodynamics and the radiation are consistently treated. The methods employed to handle the non-planar geometry, the time-dependent particle conservation equations, the departures from LTE and the radiation field are outlined. We discuss the various possible approximations in photospheric, chromospheric and coronal loop applications in late-type stars as well as the radiation pressure treatment in early-type stars.

1. Introduction

The atmospheres of stars where acoustic or magnetoacoustic waves propagate are characterized by large changes in gas density. This is due to the comparatively low stellar surface temperatures which determine the scale heights and e.g. in the sun lead to a density drop of eight orders of magnitude from the bottom of the photosphere to the top of the chromosphere, a distance of only 2500 km. This density drop has important consequences for the thermodynamic and radiative properties of the gas and thus for the wave propagation.

At the base of the photosphere the density is so large that the optical depth at all frequencies is greater than one and thus radiation (in the diffusion limit) escapes into space only with difficulty. Here particles collide frequently enough that the energy levels are populated as in local thermodynamic equilibrium (LTE); the Saha equation governs the stages of ionization, the Boltzmann distribution describes the population of the energy levels and the radiative source function is the Planck function. Since the thermodynamic and radiation properties here can be described by local quantities the wave computation is comparatively simple.

In the inner corona on the other hand, the gas density is so low that the gas is optically thin and each photon escapes. At these heights there are so few collisions that both the ionization and the level populations are determined by the individual surviving transitions (non-LTE). Owing to different heating processes the electron and ion temperatures defined by the Maxwell velocity distributions begin to show different values. The non-LTE excitation and ionization can be computed here using the thin plasma approximation which again is dependent only on local quantities. The main difficulty in the coronal situation is that due to the low gas density the degree of ionization and the population of energy levels often cannot follow instantaneously the time-dependence of the wave. The fewer the number of collisions per wave period the more the dynamical state attained by the atmosphere differs from the static situation. Thus in the coronal situation

the particle conservation equations must be solved explicitly. As this can be done by using local quantities in the thin plasma approximation the wave computation in the corona is still relatively uncomplicated.

The treatment of the acoustic wave propagation is most difficult in the intermediate chromospheric region where the simplifying assumptions of LTE and of the thin plasma approximation break down. Here the thermodynamic and radiative properties of the gas depend not only on the density and temperature but also very much on the nonlocal radiation field. In strong chromospheric resonance lines the radiation field can be trapped, leading to LTE conditions for this element, while for other elements non-LTE conditions already prevail. This situation is complicated even further by the large inhomogeneities in the stellar atmospheres where e.g. in magnetic flux tubes the gas pressure can be smaller by as much as an order of magnitude compared to the outside medium.

The discussion so far dealt primarily with the situation in late-type stars. Intense radiation fields in early-type stars lead to entirely new situations for the acoustic wave propagation. The radiative relaxation times in the photospheres of early-type stars are so small that deviations from isothermality are damped in a matter of seconds. This leads to the formation of extensive radiation damping zones around these stars. After the waves have propagated through these zones, radiation pressure rapidly amplifies the waves and strong shocks are generated. Here the radiation pressure can no longer be computed using the Sobolev approximation which has been employed in time-independent radiation-driven wind theories and which is valid when large persistent velocity gradients occur. In the photosphere and chromosphere of early-type stars the wind velocities and the velocity gradients are small and determined by the acoustic waves. Thus radiation pressure must be handled differently.

From this overview it is clear that time-dependent dynamic wave calculations which can satisfactorily deal with all of the above mentioned situations are quite difficult. It therefore becomes important to make approximations and to outline regions of the atmosphere where simplifications can be made which make the problem tractable without losing the essential physics. In the following sections we review time-dependent dynamic (magneto-) acoustic wave calculations where both the radiation field and the thermodynamics are consistently treated grouping them into classes according to the approximations typically made. These classes are defined by the way radiation is treated. Adiabatic wave calculations are omitted. For lack of space we also have omitted a discussion of the time-dependent radiation hydrodynamic calculations of granulation flows, of accretion flows onto stars or protostellar objects, of gas jets from protostellar nebulae and shocked gas flows from novae or supernovae. Even for atmospheric wave calculations we do not attempt completeness. Time-dependent nonlinear calculations of magnetoacoustic wave propagation which consistently treat radiation are so far available only for the acoustic-like longitudinal tube waves. All present acoustic wave calculations are one-dimensional.

Vernazza, Avrett and Loeser (1981) have shown that the main chromospheric emitters are the H^- continuum, the principal lines of CaII and MgII, the Lyman continuum and the Lyman α line. H^- contributes mainly in the low chromosphere and in the photosphere while Lyman emission occurs only in the high chromosphere. Deeper in the photosphere there is in addition a multitude of metal line and continuum emitters. These contributions can be

computed using Kurucz's (1979) opacity table. Wave calculations which use photospheric opacity tables or formulae and assume LTE are termed photospheric calculations and are reviewed in Section 2. Section 3 describes the coronal loop calculations where the optically thin radiation can be treated comparatively simply but where the time-dependent particle conservation equations must be considered. Computations where the non-grey radiation field is taken fully into account and where the time-dependent particle conservation equations are consistently treated but where only Lyman emission and plane geometry are considered have been termed high chromosphere calculations and are discussed in Section 4. Section 5 describes low and middle chromosphere calculations. Here non-grey H^- as well as MgII and CaII line emission are taken into account, the particle conservation equation is solved and flux tube geometry effects are considered. Acoustic wave calculations in early type stars where radiation pressure is important and an intense energy exchange with the photospheric radiation field occurs is discussed in Section 6. Section 7 gives a summary and a discussion.

2. Photospheric calculations

A simple type of radiation treatment is possible in work which we call photospheric calculations. Typical examples of such work are that of Hasan and Schüssler (1985), Herbold et al. (1985), Leibacher, Gouttebroze and Stein (1982), Stein and Schwartz (1972) as well as Ulmschneider et al. (1978). Here one assumes either a neutral or an ionizing gas of mean molecular weight μ where the thermodynamic state and the radiative source function can be computed assuming LTE. The thermodynamic state of the gas is described by the ideal gas equation

$$p = \varrho \frac{RT}{\mu} \quad , \tag{1}$$

where p is the gas pressure, ϱ the density, R the universal gas constant and T the temperature.

a. hydrodynamic equations

The (magneto-) acoustic wave propagation in one dimension is governed by the following set of hydrodynamic equations (c.f. Hirschfelder, Curtiss, Bird 1954, pp. 462, 701, Landau, Lifshitz 1959, p. 2ff) :

the continuity equation

$$\frac{\partial}{\partial t}(\varrho A) + \frac{\partial}{\partial x}(\varrho u A) = 0 \quad , \tag{2}$$

the Euler equation

$$\varrho\left(\frac{\partial u}{\partial t} + u \frac{\partial u}{\partial x}\right) + \frac{\partial p}{\partial x} + \varrho g = 0 \quad , \tag{3}$$

the energy equation

$$T\left(\frac{\partial S}{\partial t} + u\,\frac{\partial S}{\partial x}\right) = -\frac{\Phi_R}{\varrho} \quad , \tag{4}$$

where t is the time and x is the height in the atmosphere. If tube geometries are considered x is the length along the tube axis. A is the cross sectional area of the tube, u the gas velocity, S the entropy per gram. g is the gravitational acceleration which usually is a constant. g is the component parallel to the tube axis in cases where tubes are considered which are inclined with respect to the vertical. For extended atmospheres, $g = g_o x_o^2/(x+x_o)^2$ where subscript 0 indicates values at the inner shell radius. Φ_R is the net radiative cooling rate in erg $cm^{-3}s^{-1}$. Effects due to molecular diffusion are neglected.

In some calculations viscosity is taken into account with corresponding additional terms in the momentum and energy equations, as we will discuss in the next section. Viscosity and thermal conductivity are important for the hydrodynamic shock structure which extends over distances of a molecular mean free path. In acoustic wave calculations the molecular mean free path is usually much smaller than the wavelength. The hydrodynamic shock can therefore be well described by a discontinuity at which the pre- and postshock states are connected via the Hugoniot relations. The radiative shock structure is usually much larger and must be explicitly treated. In photospheric and chromospheric wave calculations it is found that outside the hydrodynamic shock structure regions both viscosity and thermal conductivity are unimportant and can be neglected (Stein and Leibacher 1974).

The hydrodynamic equations must be augmented by an equation which relates the entropy to the other thermodynamic variables. For neutral or fully ionized gases one has

$$S = S_o + \frac{1}{\gamma-1}\,\frac{R}{\mu}\ln(p\varrho^{-\gamma}) \quad , \tag{5}$$

where S_o is an arbitrary constant and $\gamma = 5/3$ is the ratio of specific heats. In cases where an ionizing gas is considered the entropy is a more complicated function (c.f. Wolf 1983, 1985a, Baschek and Scholz 1982, p.122) and it becomes cumbersome to use the energy equation in the form (4). Here suitable form of Eq. (23) is used.

b. numerical methods

Several numerical methods were employed to solve the above system of partial differential equations. A most commonly used scheme is the leapfrog type finite difference method using a fixed monotonic grid spacing and using pseudo-viscosity (von Neumann and Richtmyer 1950 see also Richtmyer and Morton 1967). The method treats shocks by the application of pseudo-viscosity so that the jumps of the physical variables occur continuously over about four grid points. The thermodynamic variables in this staggered

mesh method are defined at cell centers and the radiative transfer equation can be solved as soon as these variables are known at the new time steps. Here the scheme can be solved explicitly or implicitly.

One improvement on this scheme is the finite difference method with an adaptive mesh (Tscharnuter and Winkler 1979, Winkler, Norman and Newman 1984, Dorfi and Drury 1986). Here an additional equation is used to continuously modify the grid spacing such that regions with large changes in the physical variables are automatically well resolved in space. In this scheme the solution is obtained implicitly employing Newton-Raphson techniques and resolutions of 10^{-8} have been claimed. Adaptive mesh techniques show great promise for one-dimensional problems but have not yet been applied to wave calculations in stellar atmospheres.

Another improvement of the fixed grid finite difference method is the flux corrected transport method developed by Boris and Book (1976, see also Book 1981). This method solves the hydrodynamic equations in the conservation form and is especially designed to conserve transporting physical quantities across the spatial grid by correcting numerical diffusion errors nonlinearly at every time step. The method is well suited to treating steep gradients such as shocks because it avoids the use of artificial viscosity.

The fourth method used in stellar atmospheric wave calculations is the modified method of characteristics developed by Hartree (1952, see also Lister 1960 and Hoskin 1964). Here the hyperbolic system of hydrodynamic differential equations is transformed into a system of ordinary differential equations along the characteristic directions. In this scheme shocks can be treated as discontinuities where the Hugoniot relations connecting the physical variables of the pre- and postshock regions are explicitly solved. With minor modifications the pre- and postshock regions can be arbitrarily spatially resolved without decreasing the time step and the shock path is explicitly followed. The radiative transfer equation at the new time step is solved by implicit iteration.

Hammer and Ulmschneider (1978) have made a comparison of the finite difference method and the characteristics method for the case of acoustic wave propagation. They find that the characteristics method with natural spline interpolation is more efficient as defined by the amount of numerical (computational) labour necessary for a given accuracy. Naturally this depends somewhat on the application at hand.

c. geometry

There are various ways in which the cross section A can be chosen:

$$A = \text{const.} \quad , \tag{6}$$

$$A = (x+x_0)^2/x_0^2 \quad , \tag{7}$$

$$A = A(x) \quad , \tag{8}$$

$$A = \phi_M/(8\pi(p_{EX}(x)-p(x,t))^{1/2} \quad . \tag{9}$$

If A is constant one has ordinary acoustic waves in a plane-parallel atmosphere. Using Eq. (7) one has acoustic tube waves in a spherically

symmetric and with Eq. (8) in an arbitrarily varying medium. Eq. (9) describes the cross sectional variation for longitudinal magnetohydrodynamic tube waves in the thin tube approximation (see e.g. Herbold et al. 1985). Here $\Phi_M = BA$ = constant is the magnetic flux along the tube, B being the magnetic field strength, and $p_{EX}(x)$ is a specified time-independent external pressure. It is seen that Eq. (9) represents the horizontal pressure balance equation

$$p + \frac{B^2}{8\pi} = p_{EX}(x) \quad . \tag{10}$$

d. radiation

In the photospheric calculations the following expressions for the net radiative cooling rate have usually been used:

$$\Phi_R = -4\pi K(J-B) \quad , \tag{11}$$

$$\Phi_R = -4\pi K(\sigma T_{EX}^4(x)/\pi - B) \quad , \tag{12}$$

$$\Phi_R = -16K\sigma T^3 \Delta T \quad , \tag{13}$$

$$\Phi_R = -4\pi K \frac{1}{3}\frac{d^2 B}{d\tau^2} \quad , \tag{14}$$

where K is the grey opacity without scattering. K as function of T and p is usually taken from tables given by Kurucz (1979). As the main contribution to the photospheric opacity is H^-, approximate formulae like

$$K = 1.376\ 10^{-23} p^{0.738} T^5 \varrho \quad , \tag{15}$$

by Ulmschneider et al. (1978) or a similar formula by Stein (1966) can often be used.

$$B = \sigma T^4/\pi \quad , \tag{16}$$

is the frequency integrated Planck function. J in Eq. (11) is the frequency integrated mean intensity and is usually obtained as solution of the grey LTE radiative transfer equation,

$$\mu\frac{dI}{d\tau} = I-B \quad , \tag{17}$$

where I is the frequency integrated specific intensity. μ is the angle cosine, τ with

$$d\tau = -K dx \quad , \tag{18}$$

is the grey optical depth which now includes scattering and

$$J = \frac{1}{2}\int_{-1}^{+1} I\,d\mu \quad . \tag{19}$$

In cases where waves along thin intense magnetic flux tubes are considered the gas pressure inside the tube is substantially less than the outside pressure. Here the tube can be considered as optically thin with the mean intensity J in the tube originating entirely from the outside medium. Thus in Eq. (12) J can be determined from the external temperature $T_{EX}(x)$. In cases where in an optically thin medium the mean intensity does not deviate much from the Planck function, Eqs. (12) and (16) may be expanded and one obtains Eq. (13). This so called Newton's law of cooling is only applicable for waves of small amplitude. For optically thick cases, expanding the Planck function with respect to τ and using Eqs. (17) and (19) one obtains the diffusion approximation Eq. (14). This approximation is only valid in regions of optical depth larger than one. A good radiative transfer calculation using Eq. (11) not only reproduces the optically thin approximation but also the diffusion approximation at great depth.

e. results

Photospheric wave calculations have been made to study four types of problems: the solar five minute oscillations, the heating mechanism and the emission of chromospheres, the structure of the temperature minimum region and the secular mass motion in downflows. The solar five minute oscillations discovered by Leighton (c.f. Noyes and Leighton 1963) are now recognized as nonradial pulsations of high angular degree l by the solar envelope. Observations show that these waves exhibit 90 degree phase shifts between the velocity and temperature fluctuations and thus demonstrate a standing wave behaviour.

With a plane nonlinear time-dependent wave calculation taking ionization into account and a radiation loss similar to Eq. (13) Leibacher (1971) investigated the propagation, the phase relationships, and the resonance behaviour of the five minute oscillations. The numerical method used to solve the hydrodynamic equations was a finite difference method with monotonic grid spacing. He found that in the solar interior these waves propagate in a cavity which is bounded at great depth by reflection from the steep temperature increase and at the photosphere by the reflection at the point where the acoustic cut-off frequency rises to equal the wave frequency. Fig. 1 shows a similar investigation by Leibacher, Gouttebroze and Stein (1982) in which with a piston motion of five cycles of five minute period the chromospheric three minute oscillations were excited. This oscillation arises in a cavity bounded below by the peak of the cut-off frequency near the temperature minimum and above by the high chromospheric temperature rise.

The second type of investigation aims to identify the solar chromospheric heating mechanism and to explain the chromospheric emission. Here short-period acoustic waves with periods below about one minute are found to be very promising. These waves have essentially no phase shifts and thus unlike the five minute oscillations can easily propagate and carry energy through the temperature minimum. First exploratory wave calculations for a wide range of acoustic pulses with periods ranging from 25 to 400 sec were made by Stein and Schwartz (1972, 1973) using a finite difference method with

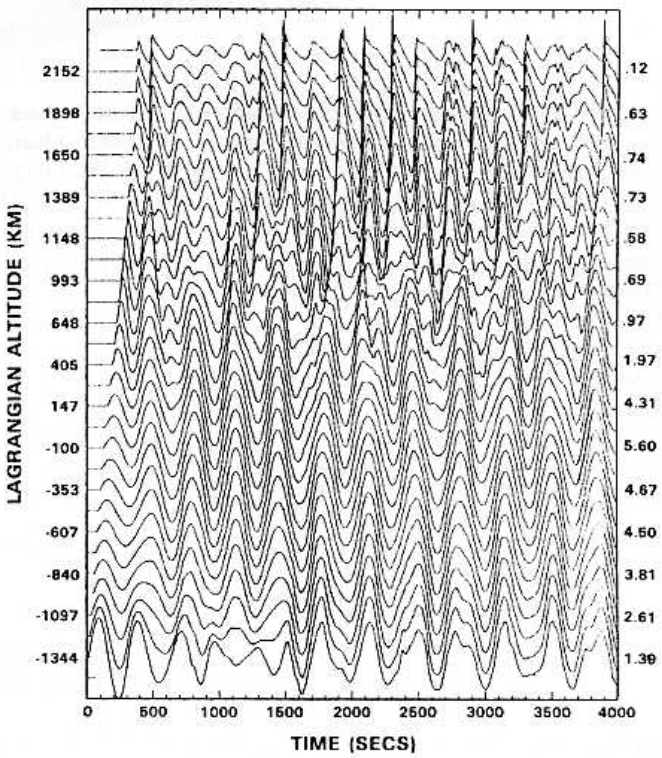

Fig.1 Simulation of the chromospheric three minute oscillations after Leibacher, Gouttebroze and Stein (1982). Shown is the square root of the kinetic energy density.

fixed grid spacing. Ionization was included and radiation was taken into account in an optically thin approximation as in Eq. (41). As an unbalanced cooling law like Eq. (41) leads to a secular change of the initial atmosphere a heating term had to be added to make the initial model time-independent. The calculations of Stein and Schwartz showed that the weak shock theory is valid for pulse periods less than 50 s and is invalid for periods greater than 100 s.

Using a numerical method and a radiation treatment like that of Stein and Schwartz, Cram (1976) made a similar calculation to investigate the time-dependent formation of the CaII K and infrared triplet λ8542 lines. An acoustic wave with a period of 200s was computed. Using the time sequence of the temperature, pressure and velocity distributions obtained from this calculation, the CaII line profiles were subsequently computed assuming complete redistribution. For this the electron density from the hydrogen ionization was calculated taking a time-independent departure coefficient b_1 as function of height. These computations were used to explain the K-grain, small bright CaII K-line emission features observed within the supergranulation cells.

In the short-period wave calculations of Ulmschneider et al. (1977,1978) a modified characteristics method was used to solve the hydrodynamic equations and to treat the shock discontinuities. Ionization effects were not taken into account. The radiative transfer equation in the grey approximation

(Kalkofen and Ulmschneider 1977) was solved simultaneously and the radiative cooling rate computed using Eq. (11). These authors found that the temperature minimum occurs close to the point of shock formation and is strongly dependent on the wave energy. The higher the wave energy flux is, the lower the height of the temperature minimum. It was demonstrated that shock formation readily explains the magnitude and sudden onset of the chromospheric radiation loss above the temperature minimum as inferred from empirical solar models. For longer period waves less shock dissipation and more mass motion was found. These calculations were extended to other late type stars (summarized by Ulmschneider 1979). Observations showed however that acoustic wave calculations which do not take into account the presence and geometrical shape of the magnetic fields only very poorly explain the chromospheric heating.

In the work of Bohn and Stein (1985) the interaction of short-period acoustic waves and five minute oscillations was investigated. These authors used a hydrodynamic code similar to that of Leibacher, Gouttebroze and Stein (1982). At the base of the solar photosphere they introduced a series of monochromatic wavetrains of different period and random duration with random phase changes together with a 300 s type oscillation. It was found that the frequency power spectrum, which at the base of the photosphere is essentially a multiple delta function, became flat and continuous at great height. In addition the calculations suggested that the acoustic heating by a spectrum of waves is more efficient than by a monochromatic wave.

A third type of time-dependent photospheric calculations aims to clarify the structure of the solar temperature minimum region. Muchmore and Ulmschneider (1985), Muchmore, Kurucz and Ulmschneider (1986) as well as Muchmore (1986) have investigated the influence of CO molecules on the time-dependent formation of radiative equilibrium atmospheres. These authors used the same numerical method as Ulmschneider et al. (1978), treating CO in LTE and solving a two-frequency radiative transfer problem. In the more recent calculations both H^- and CO were treated non-grey, the latter with opacity distribution functions. Fig. 2 shows that stars with an effective temperature T_{eff} less than about 5800 K have radiative equilibrium atmospheres with cool outer layers. Acoustic shock heating can limit these cold regions from above. In the range of T_{eff} between 5800 and 5900 K, depending on the previous history of the atmosphere, two types of radiative equilibrium atmosphere can actually occur, a cold one dominated by CO cooling or a hot one.

The structure of the temperature minimum area is dominated on the one hand by extensive cold regions and on the other by intensely heated magnetic flux tubes which penetrate the cold regions. In their wave calculations along flux tubes Herbold et al. (1985) solved the hydrodynamic equations and the modified Hugoniot relations using the characteristics method. They took various geometries (Eqs. 6,8,9) and radiation loss after Eq. (12) to compute ordinary acoustic waves, acoustic tube waves and longitudinal magnetohydrodynamic tube waves. The method of characteristics was taken and ionization was neglected. It was found that acoustic tube waves and longitudinal waves are very similar due to the dominant influence of the tube spreading.

A fourth type of photospheric calculation is represented in the work of Hasan and Schüssler (1985). These authors computed the time development of a downward gas flow in a solar flux tube. Here hydrogen ionization was taken

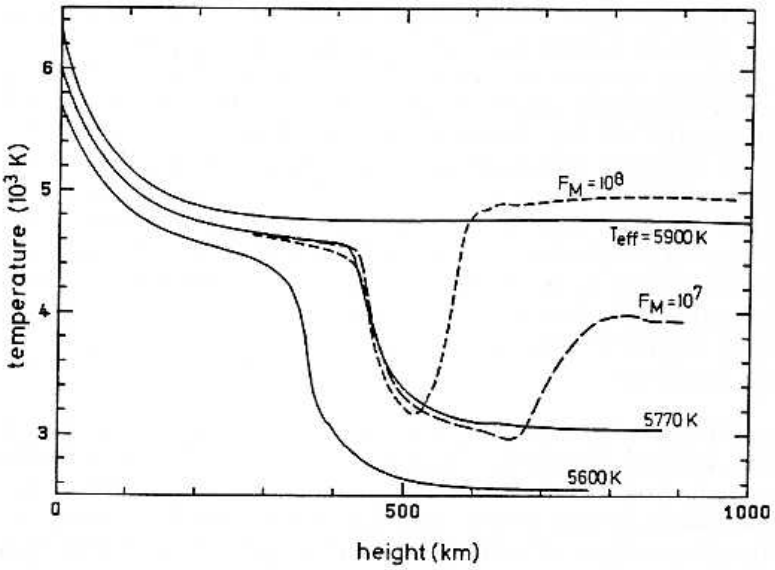

Fig.2 Temperature structure in radiative equilibrium models for various effective temperatures T_{eff} obtained in a time-dependent calculation after Muchmore and Ulmschneider (1985). Models with acoustic heating are shown dashed. The acoustic flux F_M is given in erg $cm^{-2}s^{-1}$.

into account and radiation after Eq. (13). The hydrodynamic equations were solved using the flux corrected transport algorithm. The initial model assumed a small downflow. The heating phase was initiated by an enhanced downflow entering at the top of the tube. It was found that the enthalpy energy flux strongly heats the tube. Good agreement with empirical flux tube models could be obtained.

3. Coronal loop calculations

Another type of calculation where the radiation treatment is comparatively simple is that along coronal loops. Typical examples of such work are Nagai(1980), Mariska and Boris (1983) and McClymont and Canfield (1983). These authors assume a fully or nearly fully ionized medium. In some work a difference between the heavy particle temperature T_H (the energy exchange by ion-neutral collisions appears rapid enough) and the electron temperature T_E is allowed for.

a. hydrodynamic equations

The continuity (2) and Euler equation (3) are not modified although the latter is often written as a momentum conservation equation (Landau, Lifshitz 1959, p. 13)

$$\frac{\partial}{\partial t}(\varrho u A) + \frac{\partial}{\partial x}(\varrho u^2 A) + A\frac{\partial p}{\partial x} + \varrho A g_P = A F_{vis} \quad , \qquad (20)$$

where the total pressure p is the sum of the electron and heavy particle pressures, g_P is the gravitational acceleration parallel to the loop axis, and F_{vis} is the viscous force, i.e. the tensor divergence of the viscous stress tensor. Cox and Everson (1983) gave the form for the viscous force in general coordinate systems and Hasan and Schüssler (1985) discussed it in detail for circular cylindrical coordinates. For the tube geometry

$$F_{vis} = [\ \frac{4}{3}\lambda\ \mathrm{grad}(\mathrm{div}(\underline{u})) - \frac{2}{3}(\mathrm{grad}\lambda)(\mathrm{div}(\underline{u}))$$

$$+ 2\ \mathrm{grad}(\lambda)\cdot\mathrm{grad}(\underline{u})\ ]_x \quad , \qquad (21)$$

where $\underline{u}$ is the velocity vector and λ is the coefficient of viscosity. This is, to good approximation,

$$F_{vis} = \frac{4}{3}\lambda\frac{\partial}{\partial x}[\frac{1}{A}\frac{\partial}{\partial x}(uA)] + \frac{2}{3}\frac{\partial\lambda}{\partial x}[\ 2\frac{\partial u}{\partial x} - \frac{u}{A}\frac{\partial u}{\partial x}] \quad . \qquad (22)$$

Note that for dilute monatomic gases the coefficient of bulk viscosity is zero (Hirschfelder, Curtiss, Bird 1954, pp. 503, 521) and it has been omitted here. In cases where hydrogen ionization or recombination occurs too slowly to keep pace with variations in T and p, the bulk viscosity is non-zero (Landau and Lifshitz 1959, p.304ff). In such cases the preferred treatment, however, is to augment the hydrodynamical equations with the particle conservation equations for the individual species of particles rather than to handle these effects by means of a bulk viscosity.

The value adopted for the viscosity coefficient may be the molecular viscosity (e.g. Spitzer 1962, Brezing 1965), or a turbulent viscosity (as used by Hasan and Schüssler 1985) or a pseudoviscosity (Richtmyer and Morton 1967). No matter which value is used for the viscosity, anytime its effects become significant, as for instance in shocks or for T above $2\ 10^7$K (McClymont and Canfield 1983), then it must be included consistently in both the momentum and energy equations, since physically the viscosity represents the transformation of kinetic energy into heat. Exactly the same energy lost from the velocity field must end up in the thermal energy (Cox and Everson 1983). We give the viscosity an emphasis out of proportion to its physical importance here because this consistency has frequently not been enforced in the calculations we are reviewing.

Because the proton-electron energy exchange time in the inner corona becomes appreciable compared to a wave period of a few seconds one now has two energy equations (Cannon 1974, Landau, Lifshitz 1959, p. 185, Hirschfelder, Curtiss, Bird 1954, p. 463),

the total energy conservation equation

$$\frac{\partial}{\partial t}(\varrho EA) + p\frac{\partial A}{\partial t} + \frac{\partial}{\partial x}[(\varrho E+p)uA - AK_I\frac{\partial T_H}{\partial x} - AK_E\frac{\partial T_E}{\partial x}\ ]$$

$$- \varrho uAg_P = A(\phi_V - \phi_R + \phi_M) \quad , \qquad (23)$$

and the electron energy conservation equation

$$\frac{\partial}{\partial t}(\varrho E_E A) + p_E \frac{\partial A}{\partial t} + \frac{\partial}{\partial x}[(\varrho E_E + p_E)uA - A\kappa_E \frac{\partial T_E}{\partial x}] =$$

$$+ A\gamma_{EQ}(T_H - T_E) - A\chi(H)R(H) - A\chi(He)R(He) - A\chi(He^+)R(He^+)$$

$$+ A(\phi_{VE} - \phi_R + \phi_M) \quad . \tag{24}$$

The right hand sides of the above two equations are the energies gained by inelastic processes. κ_I and κ_E are the thermal conductivities for the heavy particles and electrons, respectively (κ_I is only 4 percent of κ_E c.f. Ulmschneider 1970, Nowak and Ulmschneider 1977). To take into account that the thermal conductive flux can not be made arbitrarily large Fisher, Canfield and McClymont (1985) have modified this coefficient. Note that due to the steep temperature gradient and the strongly reduced radiation loss, thermal conductivity becomes important in the transition layer and the corona. Viscosity is important only when steep velocity gradients are produced by localized flare heating events. ϕ_V is the net viscous heating rate (Landau and Lifshitz 1959, p.184) and ϕ_{VE} is the corresponding rate for electrons. ϕ_M is a net heating rate by external processes. γ_{EQ} is a heavy particle-electron equilibration rate. $\chi(H)$, $\chi(He)$, $\chi(He^+)$ are respectively the H, HeI and HeII ionization energies. The total energy E per gram is the sum of the kinetic, heavy particle thermal, electron thermal and ionizational energies,

$$E = \frac{1}{2}u^2 + E_{INT} = \frac{1}{2}u^2 + \frac{3}{2}\frac{n_H kT_H}{\varrho} + \frac{3}{2}\frac{n_E kT_E}{\varrho} + [n(H^+)\chi(H)$$

$$+ n(He^+)\chi(He) + n(He^{++})(\chi(He) + \chi(He^+)]/\varrho \quad , \tag{25}$$

where E_{INT} is the internal energy per gram, k the Boltzmann constant and

$$n_H = n(H) + n(H^+) + n(He) + n(He^+) + n(He^{++}) \quad , \tag{26}$$

$$n_E = n(H^+) + n(He^+) + 2n(He^{++}) \quad , \tag{27}$$

where n_H, n_E, $n(H)$, $n(H^+)$, $n(He)$, $n(He^+)$, $n(He^{++})$ are the heavy particle, electron, neutral hydrogen, proton, neutral helium, ionized helium and doubly ionized helium densities, respectively. The electron energy is given by

$$E_E = \frac{3}{2}\frac{n_E kT_E}{\varrho} \quad . \tag{28}$$

The density is

$$\varrho = \mu_H m_A [n(H) + n(H^+)] + \mu_{He} m_A [n(He)$$

$$+ n(He^+) + n(He^{++})] \quad . \tag{29}$$

where μ_H and μ_{He} are the mean molecular weights of hydrogen and helium and m_A is the mass of the atomic unit. R(H), R(He), R(He^+) are the net creation rates of H, He, He^+, respectively in their ground state, obtained from Eq. (32). The terms involving these rates in Eq. (24) represent the electron energies lost by ionizing H, He, and He^+, while the term involving δ_{EQ} describes the electron energy gained from electron-heavy particle collisions. Eq. (23) except for the viscosity and thermal conduction terms can be derived from Eq. (4) by using the thermodynamic relation

$$T\frac{dS}{dt} = \frac{dE_{INT}}{dt} - \frac{1}{\varrho^2}\frac{d\varrho}{dt} \quad . \tag{30}$$

The left hand side of Eq. (30) is the external heat input. Elements other than hydrogen and helium only negligibly contribute to the thermodynamics and hydrodynamics but are important for the radiation. The work terms $p\partial A/\partial t$ and $p_E \partial A/\partial t$ vanish when the geometry is held rigid and have not been included in the calculations described below.

The viscous heating rates in the tube geometry can be approximated as

$$\phi_V = \frac{1}{A}\frac{\partial}{\partial x}\left[4/3\ \lambda\ A^{3/2}\ u\ \frac{\partial}{\partial x}(uA^{-1/2})\right] \quad , \tag{31}$$

and a corresponding term for ϕ_{VE} with λ_E replacing λ.

b. particle conservation equations

The particle conservation equations can be written (Mihalas and Mihalas 1984, p.389)

$$R_J = \frac{\delta n_J}{\delta t} = \frac{\partial}{\partial t}(n_J A) + \frac{\partial}{\partial x}(n_J u A) =$$

$$A[n_U(R_{UJ} + C_{UJ}) + n_L(R_{LJ} + C_{LJ}) + n_J^*(R_{KJ} + C_{JK})$$

$$- n_J(R_{JU} + R_{JL} + R_{JK} + C_{JU} + C_{JL} + C_{JK})] \quad , \tag{32}$$

for every level J. The right hand side must be summed over all upper U and lower L states including the continuum K. Here n_J^* is the LTE number density of level J

$$n_J^* = \frac{n_E n_I g_J}{u_I}\left(\frac{h^2}{2\pi m_E kT_E}\right)^{3/2} \exp(E_J/kT_E) \quad , \tag{33}$$

where n_I is the number density of the next higher state of ionization, u_I the partition function of this state, g_J the statistical weight of level J, and m_E the mass of the electron. The radiative and collisional rates are given by (Mihalas 1970, p.137ff):

$$R_{LK} = \int_{\nu_L}^{\infty} \alpha_L(\nu) \frac{4\pi J_\nu}{h\nu} d\nu \quad , \tag{34}$$

$$R_{KL} = \int_{\nu_L}^{\infty} \alpha_L(\nu) \frac{4\pi}{h\nu} \left(J_\nu + \frac{2h\nu^3}{c^2} \right) \exp\left(-\frac{h\nu}{kT_E}\right) d\nu \quad , \tag{35}$$

$$R_{LU} = B_{LU} \int \varphi_\nu J_\nu \, d\nu \quad , \tag{36}$$

$$R_{UL} = B_{UL} \int \varphi_\nu J_\nu \, d\nu + A_{UL} \quad , \tag{37}$$

$$C_{LK} = n_E \Omega_{LK} \quad , \tag{38}$$

$$C_{UL} = n_E \Omega_{UL} \quad , \tag{39}$$

$$C_{LU} = n_E \Omega_{LU} \quad . \tag{40}$$

Here ν is the frequency, J_ν the monochromatic mean intensity, $\alpha_L(\nu)$ the bound-free absorption cross section for level L, φ_ν the line absorption profile, B_{LU}, B_{UL}, A_{UL} are the Einstein transition probabilities, the Ω's are functions of T_E, c is the velocity of light and h Planck's constant.

For the highly ionized coronal medium the radiation fields relevant for the widely separated energetically important atomic levels are in the far UV spectral region where the intensity emitted from the much cooler stellar surface is negligibly small. The so called thin plasma approximation assumes therefore that in Eqs. (34) to (37) the intensities J_ν can be neglected. The spontaneous radiative recombination rates are then balanced by the collisional excitation rates and the particle conservation equations can be solved directly using only local values of the temperature and density. This approach has been taken e.g. by Nagai (1980), Mariska and Boris (1983) as well as by McClymont and Canfield (1983). For hydrogen where the thin plasma approximation is not very good McClymont and Canfield have used another approach. They calculate J_ν approximately with an escape probability method which corresponds to a one-frequency-point treatment and obtain a more realistic solution of Eq. (32).

c. radiation

Similar to the treatment of the particle conservation equations, there are two types of radiation treatment used in coronal loop calculations. Using the thin plasma approximation the net radiative cooling rate is only a function of T_E and density and can be written as

$$\Phi_R = n_E \, n_I \, P_{RAD}(T_E) \quad , \tag{41}$$

where P_{RAD} is a tabulated function of temperature T_E given by various authors (Cox and Tucker 1969, McWhirter et al. 1975, Rosner et al. 1978, Peres et al. 1982, Raymond 1979). This approach has been used by all workers in the field.

To improve their radiation treatment of hydrogen McClymont and Canfield

(1983) have removed the contribution of this element from Eq. (41) and have computed the mean intensity J_L and the source function S_L with an escape probability method. The net radiative cooling rate for the hydrogen contribution is then given by grey formulae (c.f. Eq. 11) of the type

$$\phi_R = -4\pi\kappa_L (J_L - S_L) \quad , \qquad (42)$$

where κ_L is a line center or continuum head opacity.

d. results

Nagai (1980), Craig and McClymont (1981), Wu et al. (1981), Mariska et al. (1982), Peres et al. (1982), Chung-Chieh Cheng et al. (1983, 1984), Mariska and Boris (1983) as well as Pallavicini et al. (1983) investigate steady and unsteady flows along coronal loops of constant or varying cross sectional area. They assume a primarily fully ionized gas and in the energy equations a Cox and Tucker type radiation loss after Eq. (41).

For their initial static models Chung-Chieh Cheng et al. (1983) and Pallavicini et al. (1983) took constant cross section loops of between 13800 and 40000 km length with base pressures between 2.9 and 6 dyn cm^{-2} as well as coronal temperatures between 10^6 and 3 10^6 K respectively. The model of the former authors assumed constant-, that of the latter authors slowly rising chromospheric temperatures. A constant height-independent mechanical heating rate ϕ_M produced by an unknown heating mechanism was adjusted such that the initial model attained a steady state. To simulate flares additional spiked pulses of mechanical heating of between 60 and 100s duration were applied to a wide region around the top of each loop. The numerical method used by Chung-Chieh Cheng et al. was the flux corrected transport method while Pallavicini et al. used the finite difference method with fixed grid spacing. Neither work explicitly solved the particle rate equations. Fig. 3 shows the resulting time development in the loop of Chung-Chieh Cheng et al., that of Pallavicini et al. showed similar time behaviour. It is seen that the pressure and the coronal temperature greatly increase. Chromospheric gas is strongly ablated and the transition layer moves from 1900 km height downward deep into the chromosphere. This leads to greatly increased radiation loss. The UV and X-ray line spectra produced by these simulations were subsequently compared with Solar Maximum Mission and P78-1 satellite observations and good overall agreement was found (Doschek et al. 1983).

The reaction of a loop model to additional steady heating or cooling and to asymmetric heating in loops of different cross sections with various spreading was investigated by Mariska et al. (1982) and by Mariska and Boris (1983). Here for the diagnostic of the oxygen lines the time-dependent particle conservation equations for this element in the thin plasma approximation were solved with the hydrodynamics. It was found that the time-dependent relative ionic abundances differed substantially from the initial equilibrium values. The loop geometry influences significantly the velocity of the induced flows. Heating may be responsible for the observed downflows.

The investigation of the flare-induced solar wind is the aim of a series of papers by Nagai (1984a,1984b) as well as Nagai and Emslie (1984) using plane, radial and nonradial tube geometries. These authors assume that the heavy

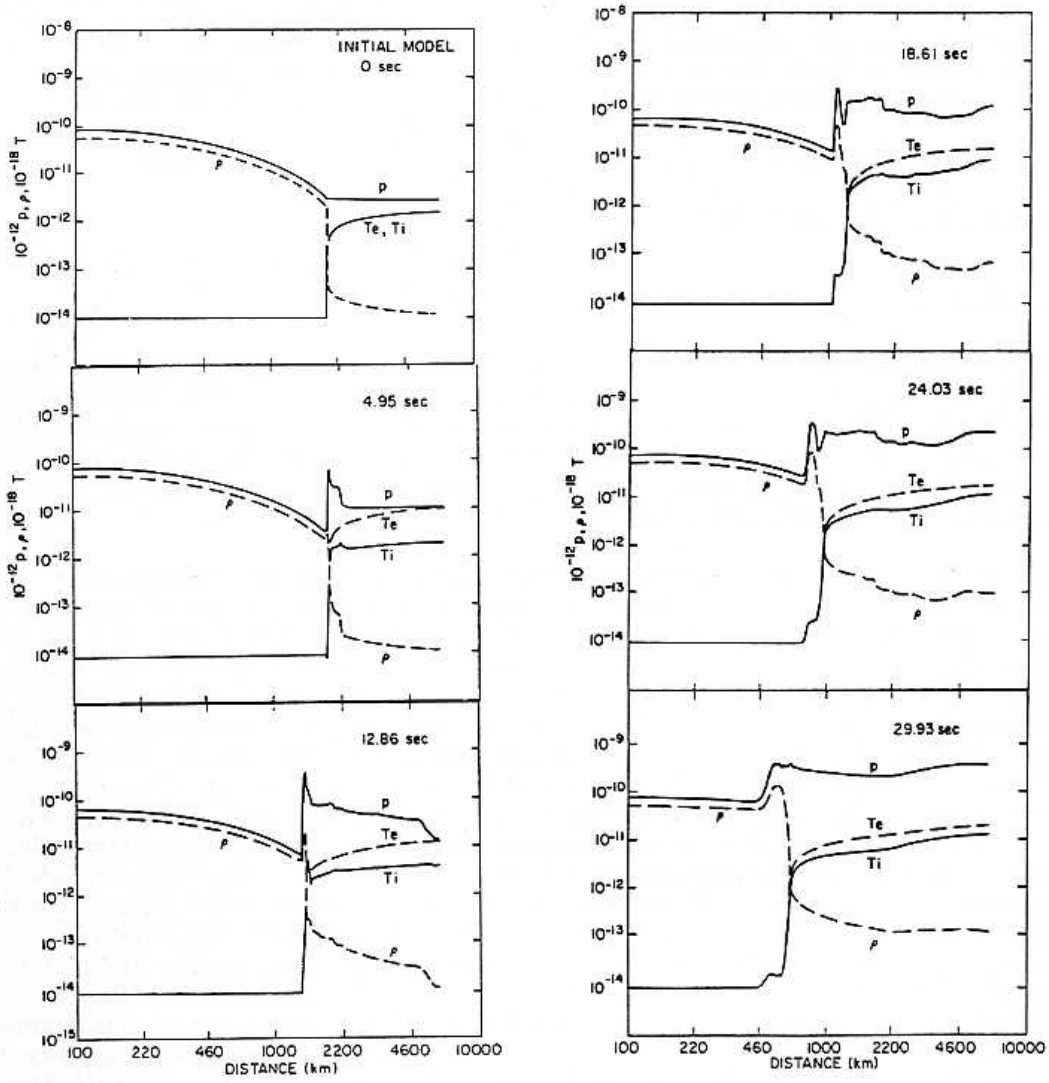

Fig.3 Time development of the gas flow in a coronal loop initiated by a flare after Chung-Chieh Cheng et al. (1983). The temperatures $T_I = T_H$, T_E, pressure p, and density ϱ for the initial model and several subsequent phases are shown.

ion and electron temperatures are equal and that the radiation loss is given by a Cox and Tucker type formula (41). Their model extends from the base of the photosphere up to 8 solar radii, well past the temperature maximum of the corona. An empirical solar atmosphere and wind model is taken as initial model. To prevent secular changes of the initial model a height-dependent heating rate $\phi_M(x)$ was applied to balance the radiative and wind losses. The flare event was simulated by a peaked additional heating rate ϕ_M of 480 sec duration and a width of 4000 km at 30000 km height. Fig. 4 shows the time development of the model where the individual phases are labelled by the time in minutes. As in the calculation of Chung-Chieh Cheng the transition layer moves deeply into the chromosphere from where it returned to its former position in about 22 min. After about 13 min a maximum flow

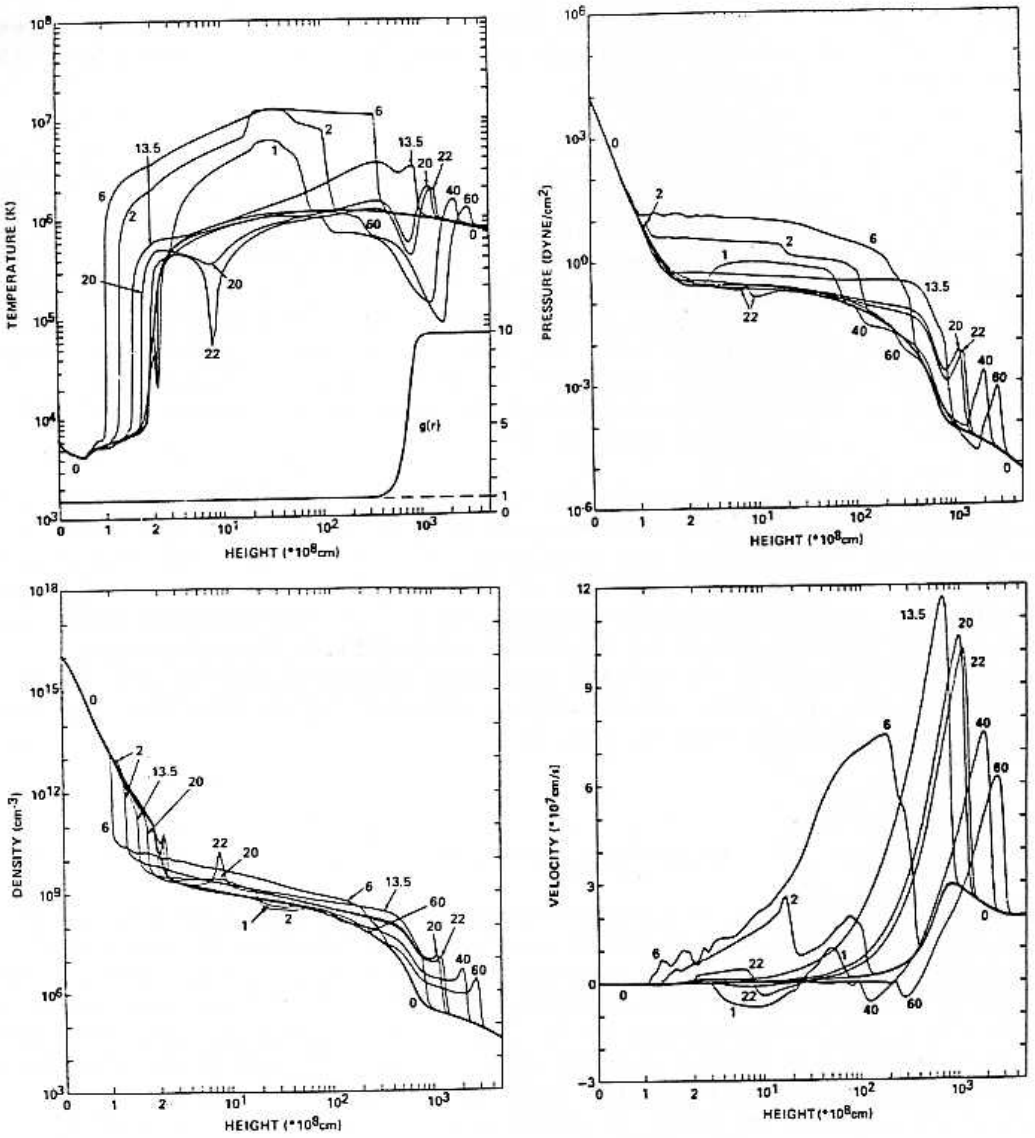

Fig.4 Time development of the gas flow in an open solar coronal flux tube initiated by a flare after Nagai (1984b). The temperature, pressure, density and velocity of various phases of the wave are shown. The parameter is the time in minutes.

velocity of 1000 km/s developed which decreased to 600 km/s after 60 min.

In the work of McClymont and Canfield (1983), An et al. (1983) as well as Fisher, Canfield and McClymont (1985) the radiation fields of the Lyman α line and the Lyman and Balmer continuum of hydrogen were explicitly treated by computation of a frequency integrated mean intensity J_L and source function S_L using an escape probability method. In the latter paper the MgII and CaII losses were improved (short of actually calculating J_L) by taking into account optical depth effects using a modified coronal approximation

which gives these losses in a form similar to Eq. (41). The authors used a finite difference method with adaptive regridding for the solution of the radiation-hydrodynamic equations.

An et al. (1983) have investigated the dynamic evolution of unstable semiempirical loop models. As the Cox and Tucker type radiation formulae (41) have a maximum of P_{RAD} around the temperature 5 10^5 K, hotter loops will be thermally unstable because a cooling perturbation will result in more emission and thus even more cooling etc. In linear stability analyses cooling times of only a few minutes were found which do not agree with the observed long-lived nature of coronal loops. In their dynamic non-linear computation An et al. found that the linear instability saturates rapidly and subsequent evolution of the loop is determined by chromospheric evaporation or condensation following the much larger coronal conductive time scale on the order of half an hour.

In the work of Fisher, Canfield and McClymont (1985) the response of coronal loops to flares with various mechanical heating rates of 5 sec duration was investigated. Fig. 5 shows the resulting time development for flares with a total mechanical energy deposition of 10^9 and 10^{11} erg cm^{-2} s^{-1}. The low energy flare produces a gentle evaporation of the chromosphere while the high energy flare produces an explosive evaporation. Here the upper chromosphere is unable to radiate the flare energy deposited and is thus rapidly heated to coronal temperatures. Interesting is also the formation of coronal condensations seen in Fig. 5.

4. High chromosphere, transition layer transients

Pure hydrogen atmospheres in plane geometry are an important regime where time-dependent solutions of the particle conservation equations and the radiative transfer equations together with the hydrodynamic equations were obtained. These applications are valid for the high chromosphere where the Lyman continuum and the Lyman α line are the most important emitters and for A-star atmospheres. As the optical depth in the vertical direction for these emitters is usually much smaller than in the horizontal direction the assumption of plane geometry is justified. In the calculations of Klein, Stein and Kalkofen (1976,1978, see also Klein 1974) and of Kneer and Nakagawa (1976) the time-dependent particle conservation equations are solved with the mean intensities J_ν taken from a radiative transfer calculation using many frequency points. The ion temperature T_H was assumed equal to the electron temperature T_E.

Klein, Stein and Kalkofen (1976) have assumed a one level plus continuum atomic model and treat the Lyman continuum explicitly. Kneer and Nakagawa (1976) have taken a two bound level plus continuum model and have treated both the Lyman continuum and the Lyman α line explicitly. The radiation field in the Balmer continuum is treated using a specified radiation temperature. For the numerical method both works use the complete linearization method and the finite difference method with fixed grid spacing.

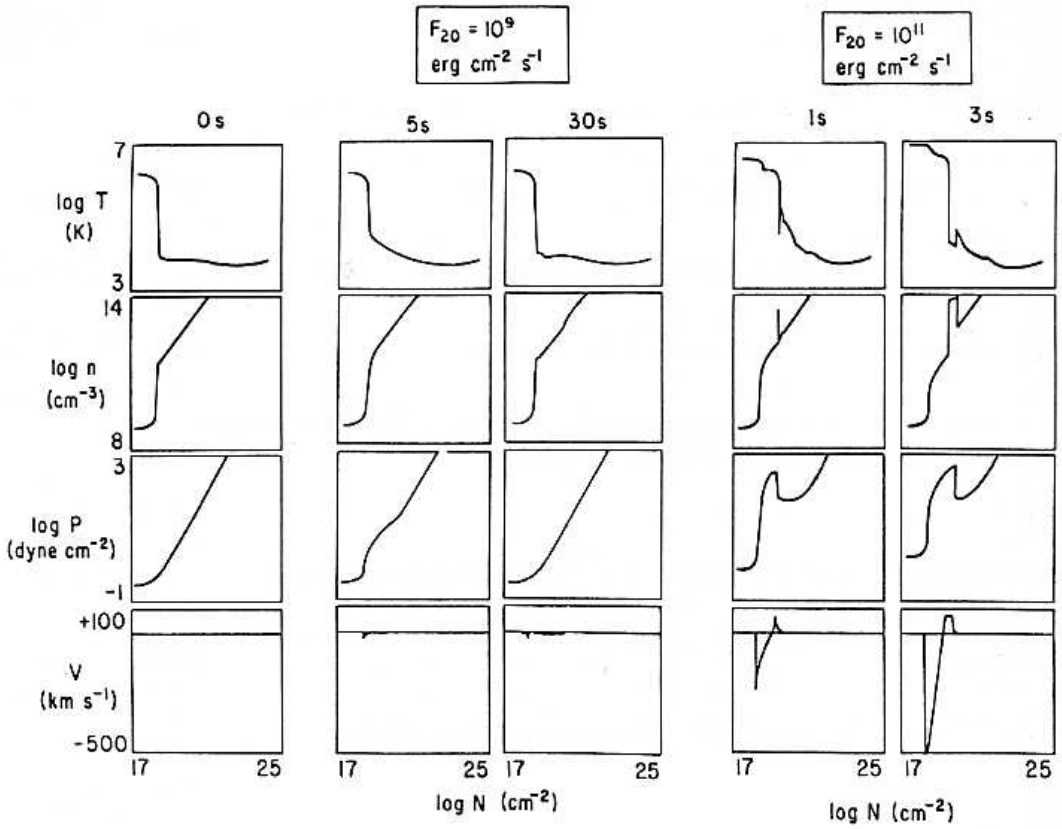

Fig.5 Time development of flares with two different energies (indicated by the heating flux F_{20}) in a coronal loop after Fisher, Canfield and McClymont (1985) showing the temperature T, numberdensity n, pressure p and velocity V. Positive velocities are downward. The initial loop model is indicated.

a. radiative transfer equation

For non-grey situations the radiative transfer equation is given by (Athay 1972, ch.2, Mihalas 1970, ch.12,13)

$$\mu \frac{\partial I_{\nu u}}{\partial x} = \eta_\nu + n_E \sigma_E J_\nu - K_\nu I_{\nu u} \quad , \qquad (43)$$

where $I_{\nu u}$ is the specific frequency and angle dependent intensity. The continuum emission coefficient is given by

$$\eta_\nu = n_1^* \alpha_1(\nu) \frac{2h\nu^3}{c^2} \exp(-\frac{h\nu}{kT}) \quad , \qquad (44)$$

with n_1^* given by Eq. (33) where $n_I = n_E$. The line emission coefficient is given by

$$\eta_\nu = n_2 A_{21} \frac{h\nu_{12}}{4\pi} \varphi_\nu \quad . \tag{45}$$

The continuum absorption coefficient is obtained from

$$K_\nu = \alpha_1(\nu)(n_1 - n_1^* \exp(-\frac{h\nu}{kT})) + n_E \sigma_E \quad , \tag{46}$$

where σ_E is the Thomson scattering cross section and

$$K_\nu = \frac{h\nu_{12}}{4\pi} B_{12} (n_1 - n_2 \frac{g_1}{g_2}) \varphi_\nu + n_E \sigma_E \quad , \tag{47}$$

is the line absorption coefficient. In these formulae complete redistribution has been assumed. Using

$$j_{\nu u} = (I_{\nu u} + I_{\nu -u})/2 \quad , \tag{48}$$

the transfer equation can be written in Feautrier form

$$\mu^2 \frac{d^2 j_{\nu u}}{d\tau_\nu^2} = j_{\nu u} - \frac{\eta_\nu}{K_\nu} - \frac{n_E \sigma_E}{K_\nu} J_\nu \quad , \tag{49}$$

where the optical depth at frequency ν is given by

$$d\tau_\nu = -K_\nu dx \quad . \tag{50}$$

This equation can be simplified using the Eddington approximation which consists of a one point angle integration:

$$\frac{1}{3} \frac{d^2 J_\nu}{d\tau_\nu^2} = J_\nu - \frac{\eta_\nu}{K_\nu} - \frac{n_E \sigma_E}{K_\nu} J_\nu \quad . \tag{51}$$

In addition to Eq. (51) suitable first order differential equations as boundary conditions at the surface and the bottom of the atmosphere must be employed.

b. radiation

The net radiative cooling rate in a medium emitting the Lyman continuum and the Lyman α line is given by

$$\phi_R = n_1^* 4\pi \int_{\nu_1}^{\infty} \alpha_1(\nu)\left(J_\nu + \frac{2h\nu^3}{c^2}\right) \exp\left(-\frac{h\nu}{kT}\right) d\nu$$

$$- n_1 4\pi \int_{\nu_1}^{\infty} \alpha_1(\nu) J_\nu \, d\nu + h\nu_{12}(n_2 A_{21}$$

$$+ n_2 B_{21} \int \varphi_\nu J_\nu \, d\nu - n_1 B_{12} \int \varphi_\nu J_\nu \, d\nu) \quad . \qquad (52)$$

c. results

In the work of Klein et al. an atmospheric slab of 20000 km extent similar to the situation in an A0 main-sequence star was considered with a surface gravity of $g=1.0\ 10^4$ g cm^{-2} and a Lyman continuum flux of 10^4 erg cm^{-2}s^{-1} entering at the bottom. The initial radiative equilibrium atmosphere is shown in Fig. 6a. The interesting feature is the outward temperature rise caused by the Cayrel effect (Cayrel 1963, 1964) which is a familiar feature in non-LTE radiative equilibrium calculations of early type stars (e.g. Auer and Mihalas 1969). This effect is caused here by the inefficiency of the radiative emission produced by the overpopulation (shown by the departure coefficient b_1) of the ground state of hydrogen. Departures from LTE start at an optical depth of $\tau_{912}=100$. In the thin outer layers the kinetic temperature of the gas is forced to higher values to increase the emission to balance the radiative absorption and satisfy radiative equilibrium. The degree of ionization X follows the temperature behaviour. The mean intensity J_L at the Lyman limit decreases and at $\tau_{912}=0.1$ attains a constant surface value.

The time-dependent acoustic wave calculation is initiated with a constant velocity piston and Fig. 6b shows the situation when the shock generated by the piston has reached the height $\tau_{912}=360$. It is seen that X, b_1 and the temperature are strongly correlated. That b_1 is strongly correlated with the temperature is explained by Eq. (32) where roughly

$$b_1 = \frac{n_1}{n_1^*} = \frac{R_{K1} + C_{1K}}{R_{1K} + C_{1K}} \quad . \qquad (53)$$

When collisional rates become small, b_1 depends mainly on the ratio of the temperature dependent rate R_{K1} and the temperature independent rate R_{1K}. It should be noted that in Fig. 6b the shock is still so deep in the atmosphere that the outer layers are not affected.

In Fig. 6c where the shock is at $\tau_{912}=83$ a precursor ionization front is generated which in subsequent times rapidly runs through the entire outer atmosphere. At a later stage Fig. 6d shows the strongly spiked shock at $\tau_{912}=0.034$ leaving a highly ionized gas region in its wake. In their subsequent paper, Klein, Stein and Kalkofen (1978) have extended their 1976 work by including the Balmer and other hydrogen continua. The lines were not considered. They find that shock radiation emerging from deep layers in the much less optically deep Balmer continuum drives an acoustic precursor wave and that the shock strength is weakened by the radiative cooling.

The work of Kneer and Nakagawa was more ambitious in that the Lyman α line

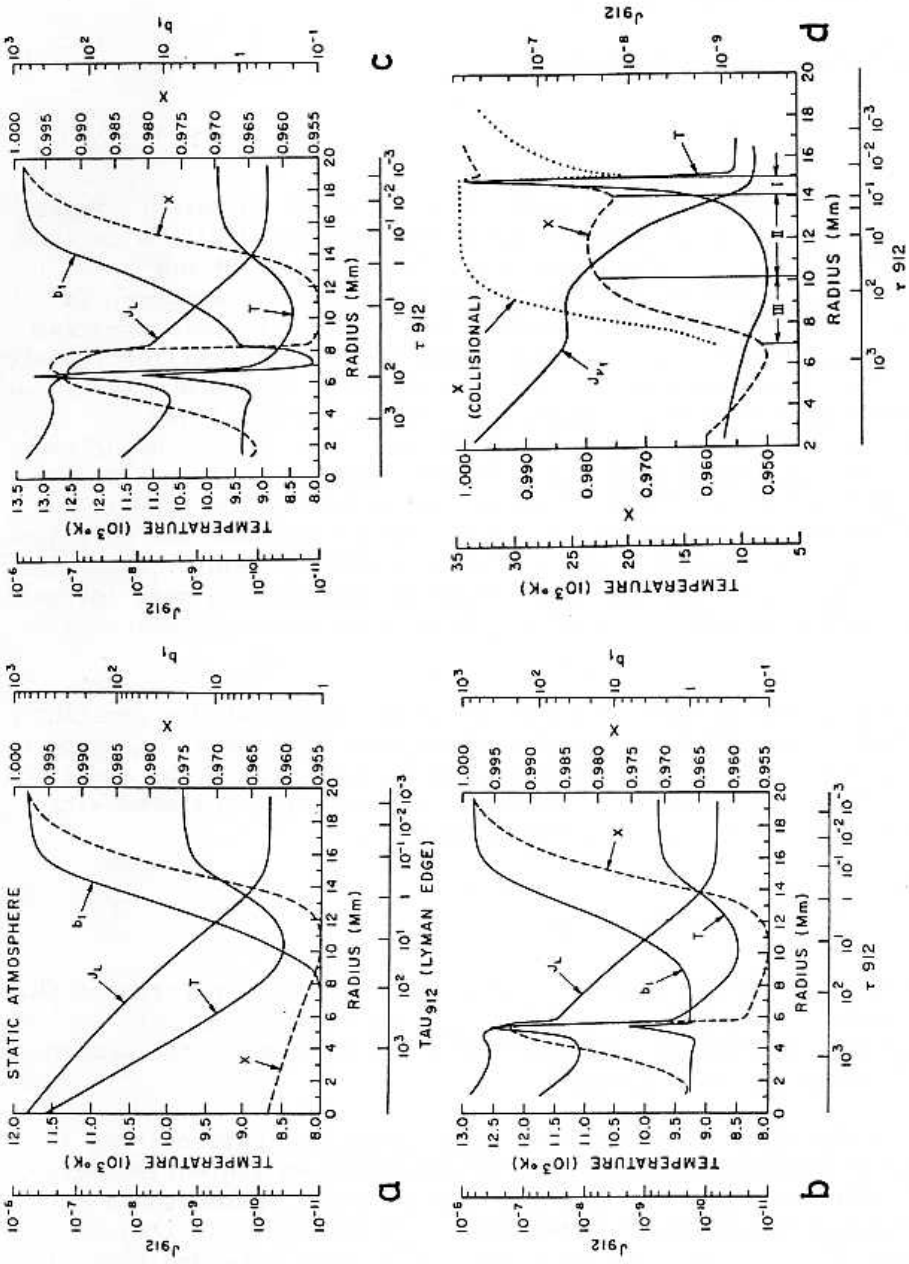

Fig.6 Development of a shock generated in an A-star type pure hydrogen atmosphere generated by a constant velocity piston after Klein, Stein and Kalkofen (1976). The initial atmosphere model and three subsequent phases are shown. T is the temperature, J_L the mean intensity at the Lyman edge, b_1 the departure from LTE coefficient and X the degree of ionization.

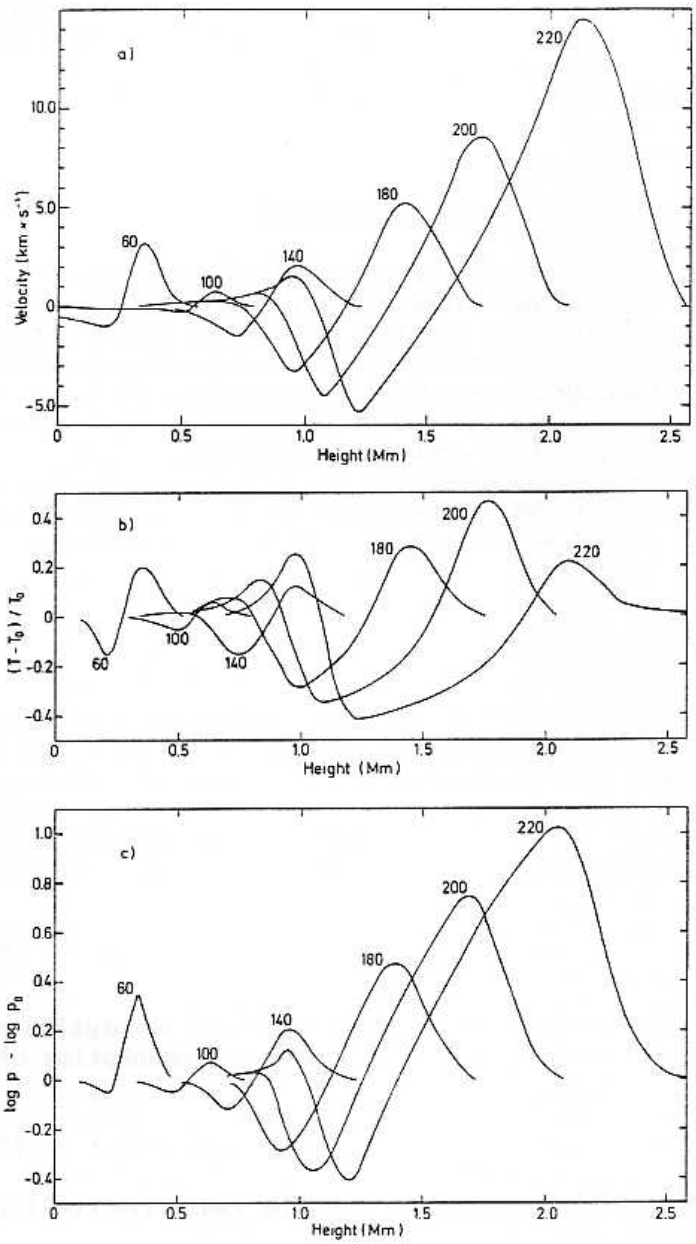

Fig.7 Time development of an acoustic pulse in the solar atmosphere after Kneer and Nakagawa (1976). The velocity, relative temperature and pressure amplitudes are shown.

was also consistently treated. In addition they took into account H^- losses in a grey optically thin, and $H\alpha$ losses in a collisional approximation. Their calculation applied to the solar chromosphere. As initial model these authors took the temperature distribution of an empirical solar atmosphere model, covering the entire 2500 km from the base of the photosphere to the transition layer. For the time-dependent computation a thermal pulse of 250 K amplitude and 25 s duration was introduced at the bottom. The time development of this pulse is seen in Fig. 7. The pulse grows to large

amplitude and moves considerable mass into the higher layers. Behind the first pulse an adiabatic cooling region develops and other pulses are generated. Although the pulse propagation is clearly seen in the Lyman α line profile the Lyman continuum showed little variation.

5. Low and middle chromosphere calculations

The important emitters in the low and middle chromosphere are the H^- continuum and the principal lines of CaII and MgII (Vernazza, Avrett and Loeser 1981). To treat these emitters adequately both non-LTE effects and resonance-line scattering effects must be taken into account. Thus, similar to the case of the high chromosphere computations, both the particle conservation equations and the radiative transfer equations must be consistently solved together with the hydrodynamic equations. In addition, for solar type stellar chromospheres the effects due to the flux tube geometry are important. We discuss here the work of Ulmschneider and Muchmore (1986) and of Schmitz et al. (1985) who use the method of characteristics.

a. H^- calculation

In the work of these authors H^- in low pressure solar flux tubes is treated in the optically thin approximation assuming a constant non-grey external mean intensity J_ν. This assumption is valid above a certain photospheric height. The particle conservation equation (32) for the one bound state of H^- was solved under the assumption that the time derivative on the left hand side is zero. The departure coefficient from LTE in H^- is then given by

$$b_- = \frac{R_{K1} + C}{R_{1K} + C} \quad , \tag{54}$$

where R_{K1} and R_{1K} are the radiative emission and absorption rates similar to Eqs. (34) and (35) where α is the H^- bound free absorption cross section and

$$C = 2\ 10^{-9} n(H) \quad , \tag{55}$$

is the neutral hydrogen collision rate. The radiative cooling rate for H^- is then given by

$$\phi_R = 4\pi \int_0^\infty (\alpha_\nu{}^{bf}(S_\nu{}^{bf} - J_\nu) + \alpha_\nu{}^{ff}(B_\nu - J_\nu))\,d\nu \quad , \tag{56}$$

where

$$S_\nu{}^{bf} = \frac{2h\nu^3}{c^2} \frac{1}{b_- \exp(h\nu/kT) - 1} \quad , \tag{57}$$

is the bound free source function and

$$B_\nu = \frac{2h\nu^3}{c^2} \frac{1}{\exp(h\nu/kT) - 1} , \qquad (58)$$

is the Planck function. ff indicates free free transitions.

b. calcium and magnesium calculations

The situation is more complicated when CaII and MgII lines are considered (Ulmschneider 1985, Ulmschneider and Muchmore 1986). In typical solar flux tubes one finds that the optical depth across the tube is much larger than along the tube. Thus a plane parallel transfer calculation should be a good approximation even for flux tubes. The authors treat only one line and assume an atomic model of two bound levels. Line scattering was computed making the assumption of complete redistribution. For the particle conservation equations it was assumed that the time dependent term at the left hand side of Eq. (32) is zero. The hydrogen ionization was not considered in the hydrodynamics but was included in LTE in the computation of the electron density for the CaII or MgII radiation treatment. The ionization of e.g. MgI to MgII and of MgII to MgIII was computed in LTE.

The net radiative cooling rate in a two level atom can be written

$$\phi_R = h\nu_{12} n_1 B_{12} \varepsilon \frac{B_{\nu 12} - S_{12}}{1 + c^2 S_{12}/2h\nu_{12}^3} , \qquad (59)$$

where $B_{\nu 12}$ is the Planck function and the photon destruction probability ε is given by

$$\varepsilon = \frac{n_E \Omega_{21}}{A_{21}} \left(1 - \exp\left(-\frac{h\nu_{12}}{kT}\right)\right) , \qquad (60)$$

and the source function by

$$S_{12} = \frac{\int \varphi_\nu J_\nu d\nu + \varepsilon B_{\nu 12}}{1 + \varepsilon} . \qquad (61)$$

The combined radiative transfer and particle conservation problem was solved using a modified core-saturation method (Kalkofen and Ulmschneider 1984) where the source function of the previous time step served as an excellent initial estimate for the new time step. To account for the neglected chromospheric emitters (MgIIh and the CaIIH+K+IRT lines) the MgIIk line results were subsequently scaled by a factor seven. In order to compare this calculation with more elaborate static computations, the chromospheric emission of model C of Vernazza, Avrett and Loeser (1981) was recomputed. The various simplifying assumptions made in the time-dependent calculation resulted in too much emission by about a factor of ten. Subsequent scaling was applied such that the Vernazza et al. results were reproduced.

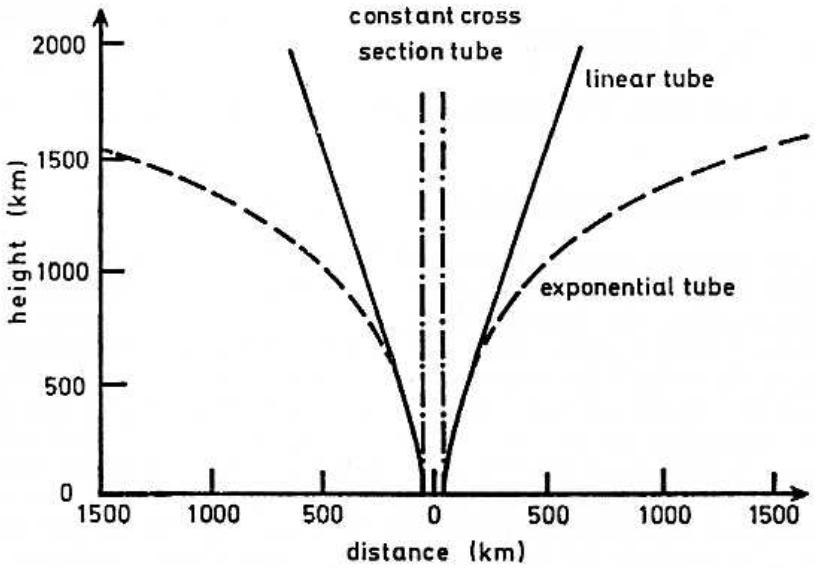

Fig.8 Types of flux tube geometry considered by Ulmschneider and Muchmore (1986)

c. results

Fig. 8 shows the three different types of flux tubes which were taken in the wave calculations. All tubes have at zero height a magnetic field strength 1500 G and a diameter 100 km. A constant cross section tube was taken. The linear tube spreads first exponentially up to 500 km and thereafter linearly. The exponential tube spreads exponentially throughout the atmosphere. Fig.'s 9, 10, 11 show calculations along the tube of constant cross section representing an ordinary acoustic wave, an acoustic wave along a linear tube, and along an exponential tube, respectively. These computations were all made with the same wave period 45 s and the same energy flux $F_M = 2.5\ 10^7$ erg $cm^{-2}s^{-1}$ which are typical values for a short-period acoustic wave.

It is seen that due to energy conservation the wave amplitudes depend strongly on the spreading of the geometry. At about 570 km height the constant case as compared to the linear and exponential cases has high temperature and velocity amplitudes. The latter two have the same amplitudes up to this height as they propagate in the same tube. At 1300 km the linear case has much larger amplitudes than the exponential case. The radiative damping function D which is related to the net radiative cooling rate by $D = -\phi_R / \varrho T$ shows that the different wave amplitudes produce large differences in emission. This is due to the fact that according to Eq. (59) both ϵ (as function of n_E) and $B_{\nu 12}$ depend strongly on temperature. The source function S_{12} is small and a slowly varying function of height. The emission is concentrated in intense radiation layers behind the shock. In front of the shock ϵ is many orders of magnitude smaller resulting in negligible absorption.

At greater height, depending on pressure and temperature, MgII is ionized to MgIII. This destruction of the only remaining emitter leads to unbalanced shock dissipation which produces a rapid rise of the mean temperature eventually resulting in a transition layer. The position of the transition

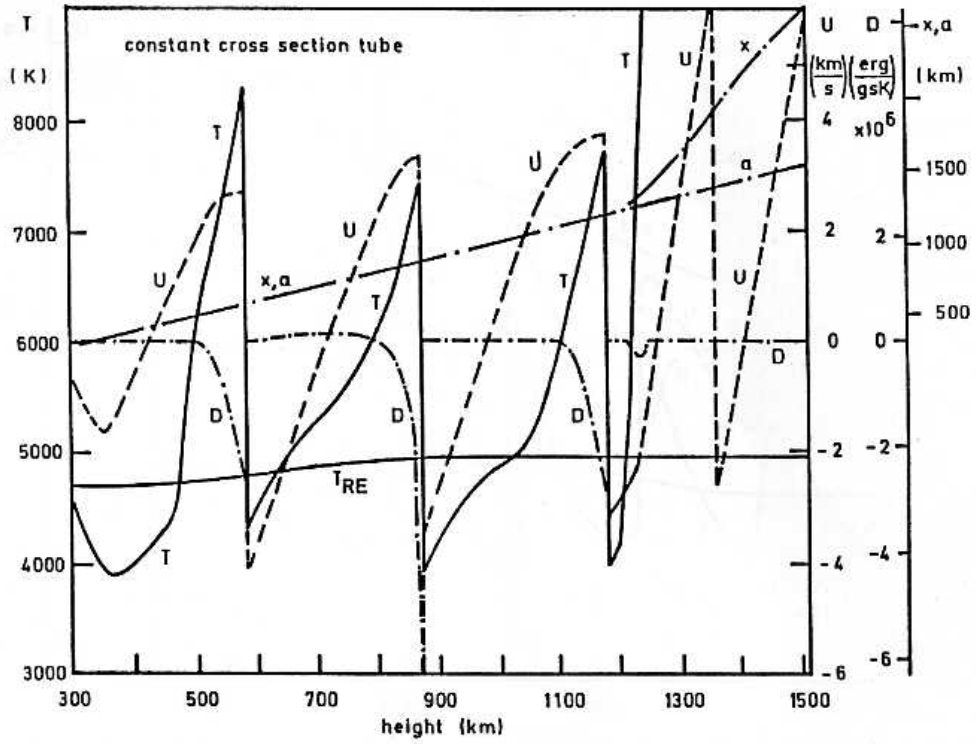

Fig.9 Temperature T, velocity u, damping function D, Euler x and Lagrange a heights for an acoustic wave in a tube of constant cross section after Ulmschneider and Muchmore (1986). T_{RE} indicates initial radiative equilibrium temperature. The wave has a period of 45 s and flux 2.5E7 erg $cm^{-2}s^{-1}$ and is shown at time 1772 s

layer depends strongly on the tube geometry, occuring at greater height the more rapidly the tube spreads. In all calculations, even those with MgII emission neglected (Schmitz et al. 1985), we found transition layers. Note that our usage of the term transition layer applies to a rapid temperature rise. The observed transition layer is probably produced by the ionization of hydrogen.

As the dissipated energy cannot be radiated away it is deposited in mass motion. Thus mass motion depends strongly on the tube geometry. This can be seen in the Figures e.g. as displacement of the Eulerian height x from the Lagrangian height a of the topmost mass point. Large mass motion is produced in the constant tube; comparatively little in the exponential tube. Long period waves put more energy into mass motion and less into chromospheric heating.

6. Calculations in early-type stars

Wolf (1985) was the first to attempt a fully nonlinear time-dependent atmospheric wave calculation in early-type stars. These stars are characterized by intense photospheric radiation fields which on the one hand are responsible for a very fast exchange of energy by radiation damping

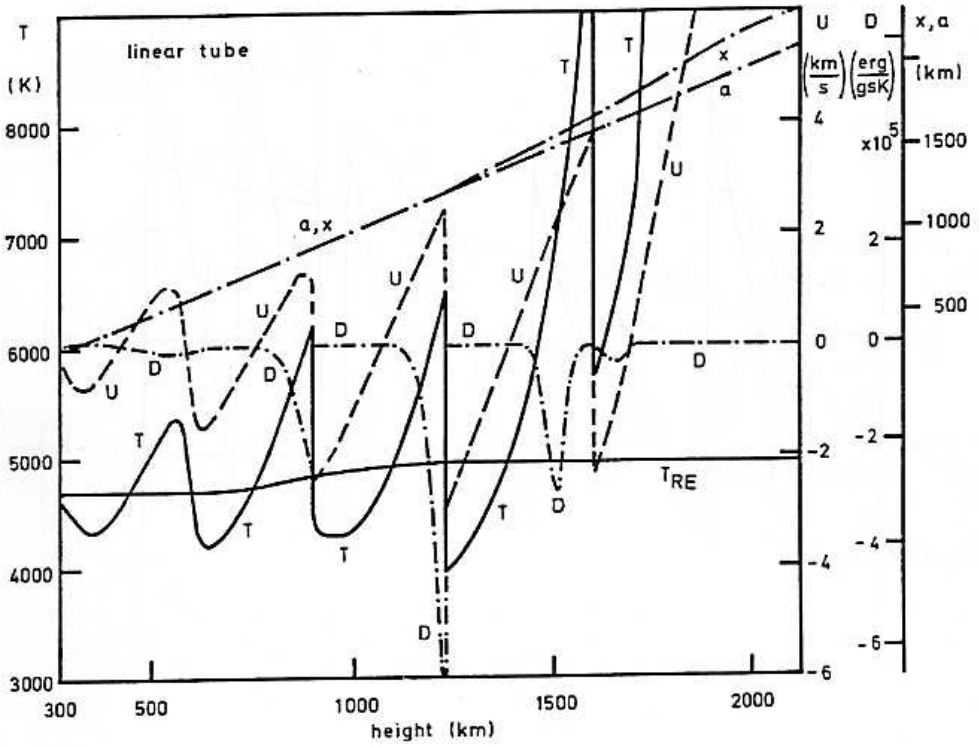

Fig.10 Same as Fig. 9 but for a linear tube at time 332 s

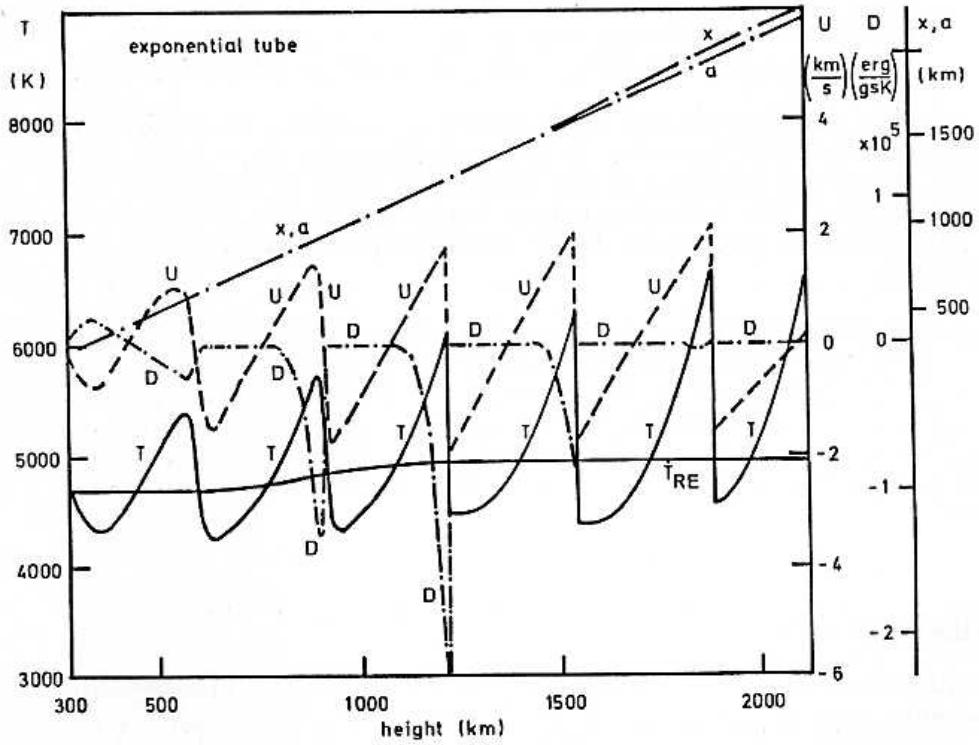

Fig.11 Same as Fig. 9 but for an exponential tube at time 693 s

and on the other for important effects due to radiation pressure. To include these effects the energy equation (4) does not need to be modified but at the left hand side of the Euler equation (3) the radiative acceleration term

$$\varrho g_R = \frac{1}{c}\int_0^\infty \kappa_\nu F_\nu \, d\nu \quad , \tag{62}$$

has to be added where F_ν is the monochromatic radiative flux. The net radiative cooling rate in Eq. (4) is given by

$$\phi_R = -4\pi\int_0^\infty \kappa_\nu (J_\nu - S_\nu)\, d\nu \quad , \tag{63}$$

where the the frequency integrations extend over the entire photospheric spectrum including lines.

a. method

To make the problem tractable Wolf (1985b) assumed LTE and rectangular line profiles and showed that Eqs. (62) and (63) can be approximated by

$$\varrho g_R = F[\kappa_R + (1-w)\kappa_1(T,p)f(u,x) + w\kappa_2(T,p) + (1-w)\sum_{i=3}^{10}\kappa_i(T,p)]/c \quad , \tag{64}$$

$$\phi_R = -4\pi\kappa_R'(J-B) \quad , \tag{65}$$

where κ_R and κ_R' are the Rosseland opacities with and without scattering, and F is the stellar radiative flux. κ_1 to κ_{10} are line opacities, f(u,x) is a function of velocity and height and w is a weighting function which decreases with height. The Rosseland opacities describe the continuum contributions. For the line contributions there are three different effects: strong resonance lines with little flux in the line core can be Doppler shifted into the continuum radiation field, weak lines contribute because there are so many of them, new ions which see an undiluted radiation field can be created by ionization in the hot compression region behind the shocks. κ_1 is the contribution from the resonance lines, κ_2 from the optically thin lines and κ_3 to κ_{10} from the strong lines of new ions. If height x=0 is the stellar surface, let $u_{MAX}(x)$ be the maximum value of the velocity of the wave in the height interval 0 to x, and $u_{MIN}(x)$ the corresponding minimum of the velocity in the same height interval, then the function f(u,x) is given by

$$f(u,x) = \begin{cases} 0 & , \text{ if } \quad u_{MIN} \le u \le u_{MAX} \\ (u-u_{MAX})/v_{th} & , \text{ if } u_{MAX} \le u \le u_{MAX}+v_{th} \\ (u_{MIN}-u)/v_{th} & , \text{ if } u_{MIN}-v_{th} \le u \le u_{MIN} \end{cases} \tag{66}$$

where v_{th} is the mean thermal speed of the line forming ions. It is seen

that f(u,x) describes the Doppler shift of resonance lines into the undiluted continuum. The contribution from the thin lines and new ions does not depend on velocity. Consider a grid point at some height x where the temperature and pressure are T and p, respectively, while at the next grid point closer to the star one has T' and p'. There are eight possibilities of T,p being greater, equal or less than T',p'. If between T',p' and T,p a new ion appears its opacity contribution is listed in the tables K_3 to K_{10}. The advantage of Wolf's approach is that the opacities K_1 to K_{10} can be pretabulated and summed over a large number of lines. Wolf took 271 lines and showed that the important contributions came from the elements H, He, C, N, O, Na, and Fe. For the numerical treatment of the hydrodynamics and the shocks Wolf used the method of characteristics and included ionization. The grey transfer equation was solved with a Feautrier type method (Wolf, Schmitz and Ulmschneider 1981) which allows for shocks.

b. results

Since the method of Wolf avoids the Sobolev approximation, it is well suited for wave calculations. A large number of wave computations for stars of spectral types O3V to A0V, B0III to B5III and O5I to B5I were made using initial acoustic fluxes corresponding to a Mach number 0.01 and periods of 0.4 the photospheric cut-off period. The calculations were started at a continuum optical depth of between 3 and 10^{-3}. It was found that there is a radiative damping zone up to an optical depth of typically 10^{-5} where the waves are essentially isothermal with a relative temperature fluctuation $\Delta T/T$ of around 10^{-7}. This also applied to the shocks formed in this zone. After passing the upper limit of the damping zone the waves rapidly grew by radiative acceleration to strong shocks with postshock temperatures of the order $3\ 10^6$ K. The generated stellar wind could not be followed because of the limited width of the atmospheric slab which extended to continuum optical depths of around 10^{-9}. The magnitude of the radiative amplification in the various stars was discussed in detail. Radiation pressure in lines was found to be the dominant contribution.

7. Conclusions

In this review we have outlined the rapid development of the capability to do nonlinear time-dependent atmospheric wave calculations in which the (magneto-) hydrodynamics, the thermodynamics and the radiation treatment are consistently coupled. The rapid decrease of the density in the atmospheres of stars introduces essentially four domains where typical wave calculations are possible:

1. High density photospheric regions where wave calculations can be done assuming LTE both for the thermodynamics and the radiation. 2. Intermediate density low and middle chromospheric regions where non-LTE effects dominate. Here the important radiation loss luckily comes from only a limited number emitters which are minority species (H^-, CaII and MgII) but the atmosphere is highly inhomogeneous and the particle conservation equations must be solved explicitly. 3. Low density high chromospheric regions at the transition layer to the fully ionized corona, where non-LTE hydrogen (Lyman continuum and Lyman α) emission dominates the radiative exchange and where the ionization of hydrogen profoundly alters the thermodynamic and radiative

properties of the gas. Here the particle conservation equations must also be solved in full detail. 4. The very low density corona where the excitation and ionization of the matter, the particle conservation as well as the radiation can be computed using the thin plasma approximation.

The great advance in storage space and speed of our present computers make it likely that one-dimensional calculations covering the entire range between the photosphere and the corona will soon be feasible. This is possible by using very efficient numerical methods to do the hydrodynamics and thermodynamics and to treat the radiation. For the treatment of non-LTE radiation the core saturation method brought a vast increase in speed as do the operator-perturbation methods of Kalkofen (1984), Scharmer (1984) as well as Scharmer and Carlsson (1985) which are claimed to be 1000 times faster than the usual complete linearization method.

Acoustic wave calculations in early-type stars have to take the intense radiative energy exchange and radiation pressure into account. Here the Sobolev approximation for the treatment of radiation pressure which is valid in cases of steep velocity gradients is no longer applicable and must be replaced by a method which allows for the three principal effects, Doppler shifting of resonance lines, weak line and new line contributions. Numerical codes are now available which are capable of treating the transition from the isothermal waves in the extensive radiation damping zones of these stars to the nearly adiabatic waves with strong developing shocks in the outer layers. Here great advances are possible if the calculations could be carried to greater heights such that the formation of the radiation-driven winds could be studied.

One-dimensional time-dependent computations of torsional and transverse Alfvèn waves along magnetic flux tubes including radiation are currently under way which could help to clarify the so far elusive coronal heating mechanism. Here the nonlinear coupling of the different MHD wave modes is especially interesting as adiabatic calculations of Hollweg, Jackson and Galloway (1982) have shown. Two-dimensional magnetohydrodynamic codes which enable more realistic treatments of flux tubes have been developed by Deinzer et al. (1984) and by Lou, Rosner and Ulmschneider (1986). It is foreseeable that these codes will use more realistic thermodynamic and radiation treatments and that they will serve as basic tools for the investigation and clarification of the chromospheric and coronal activity of stars. Another very promising area where time-dependent stellar atmospheric wave propagation will become important is the radial or nonradial pulsation-driven mass loss in late-type giant stars as adiabatic and isothermal computations of Wood (1979) show. This problem is complicated because of the great complexity of the thermodynamic and radiative treatment of molecules and dust as well as their formation. Finally the time-dependent acoustic wave computations in early-type stars are likely to play a leading role in the clarification of the radiation-driven winds from these stars.

Acknowledgement. The authors acknowledge the generous support of the Sonderforschungsbereich 132.

References

An,C.-H., Canfield,R.C., Fisher,G.H., McClymont,A.N.: 1983, Astrophys.J. 267, 421
Athay,R.G.: 1972, Radiation Transport in Spectral Lines, Reidel, Dordrecht
Auer,L.H., Mihalas,D.: 1969, Astrophys.J. 156, 681
Baschek,B., Scholz,M.: 1982, Landolt-Börnstein Series VI/2b, K.Schaifers, H.H.Voigt eds., Springer, Heidelberg, p.91
Bohn,H.U., Stein,R.F.: 1985, Proc.Workshop on Theoretical Problems in Solar Physics,Munich
Book,D.L. ed.: 1981, Finite-Difference Techniques for Vectorized Fluid Dynamic Calculations, Springer, New York
Boris,J.P., Book,D.L.: 1976, Methods Comput.Phys. 16, 85
Brezing,D.: 1965, AIAA-Journ. 3, 1422
Cannon,C.J.: 1974, J.Quant.Spectr.Rad.Trans. 14, 761
Cayrel,R.: 1963, Compt.Rend.Acad.Sci.Paris 257, 3309
Cayrel,R.: 1964, Smithsonian Astrophys.Obs.Spec.Rept. 167, 169
Cheng,C.-C., Oran,E.S., Doschek,G.A., Boris,J.P., Mariska,J.T.: 1983, Astrophys.J. 265, 1090
Cheng,C.-C., Karpen,J.T., Doschek,G.A.: 1984, Astrophys.J. 286, 787
Cox,D.P., Tucker,W.H.: 1969, Astrophys.J. 157, 1157
Cox,J.P., Everson,B.L.: 1983, Astophys. J. Suppl. 52, 451
Craig,I.J.D., McClymont,A.N.: 1981, Solar Phys. 70, 97
Cram,L.E.: 1976, Astron.Astrophys. 50, 263
Deinzer,W., Hensler,G., Schüssler,M., Weisshaar,E.: 1984, Astron.Astrophys. 139, 426
Dorfi,E.A., Drury,L.O'C.: 1986, J.Comput.Phys. in press
Doschek,G.A., Cheng,C.-C., Oran,E.S., Boris,J.P., Mariska,J.T.: 1983, Astrophys.J. 265, 1103
Fisher,G.H., Canfield,R.C., McClymont,A.N.: 1985, Astrophys.J. 289, 414
Hammer,R., Ulmschneider,P.: 1978, Astron.Astrophys. 65, 273
Hartree,D.R.: 1952, Los Alamos Report LA-HU-1
Hasan,S.S., Schüssler,M.: 1985, Astron.Astrophys. 151, 69
Herbold,G., Ulmschneider,P., Spruit,H.C., Rosner,R.: 1985, Astron.Astrophys. 145, 157
Hirschfelder,J.O., Curtiss,C.F., Bird,R.B.: 1954, Molecular Theory of Gases and Liquids, Wiley, New York
Hollweg,J.V., Jackson,S., Galloway,D.: 1982, Solar Phys. 75, 35
Hoskin,N.E.: 1964, Methods Comput.Phys. 3, 265
Kalkofen,W.: 1984, Methods in radiative transfer, W.Kalkofen ed., Univ.Press, Cambridge, p.427
Kalkofen,W., Ulmschneider,P.: 1977, Astron.Astrophys. 57, 193
Kalkofen,W., Ulmschneider,P.: 1984, Methods in radiative transfer, W.Kalkofen ed., Univ.Press, Cambridge, p.131
Klein,R.I.: 1974 Ph.D.thesis, Brandeis Univ., Waltham, Mass.
Klein,R.I., Stein,R.F., Kalkofen,W.: 1976, Astrophys.J. 205, 499
Klein,R.I., Stein,R.F., Kalkofen,W.: 1978, Astrophys.J. 220, 1024
Kneer,F., Nakagawa,Y.: 1976, Astron.Astrophys. 47, 65
Kurucz,R.: 1979, Astrophys.J.Suppl. 40, 1
Landau,L.D., Lifshitz,E.M.: 1959, Fluid Mechanics, Pergamon, London
Leibacher,J.W.: 1971, Ph.D. thesis, Harvard Univ., Cambridge, Mass.
Leibacher,J., Gouttebroze,P., Stein,R.F.: 1982, Astrophys.J. 258, 393
Lister,M.: 1960, in Math.Methods for Digital Computers 1, A.Ralston, H.S.Wilf eds., Wiley, New York, p.165
Lou,Y.Q., Rosner,R., Ulmschneider,P.: 1986, Astrophys.J. to be published
Mariska,J.T., Boris,J.P.: 1983, Astrophys.J. 267, 409

Mariska,J.T., Boris,J.P., Oran,E.S., Young,T.R.Jr., Doschek,G.A.: 1982, Astrophys.J. 255, 783
McClymont,A.N., Canfield,R.C.: 1983, Astrophys.J. 265, 483
McWhirter,R.W.P., Thonemann,P.C., Wilson,R.: 1975, Astron.Astrophys. 40, 63
Mihalas,D.: 1970, Stellar Atmospheres, Freeman, San Fransisco
Mihalas,D., Mihalas,B.W.: 1984, Foundations of Radiation Hydrodynamics, Univ.Press, Oxford
Muchmore,D.: 1986, Astron.Astrophys. in press
Muchmore,D., Ulmschneider,P.: 1985, Astron.Astrophys. 142, 393
Muchmore,D., Kurucz,R., Ulmschneider,P.: 1986, Astron.Astrophys. to be published
Nagai,F.: 1980, Solar Phys. 68,351
Nagai,F.: 1984a, Astrophys.J. 277, 379
Nagai,F.: 1984b, Astrophys.J. 278, 841
Nagai,F., Emslie,A.G.: 1984, Astrophys.J. 279, 896
Nowak,T., Ulmschneider,P.: 1977, Astron.Astrophys. 60, 413
Noyes,R.W., Leighton,R.B.: 1963, Astrophys.J. 138, 631
Pallavicini,R., Peres,G., Serio,S., Vaiana,G., Acton,L., Leibacher,J., Rosner,R.: 1983, Astrophys.J. 270, 270
Peres,G., Rosner,R., Serio,S., Vaiana,G.S.: 1982, Astrophys.J. 252, 791
Raymond,J.C.: 1979, Astrophys.J.Suppl. 39, 1
Richtmyer,R.D., Morton,K.W.: 1967, Difference Methods for Initial-Value Problems 2nd ed., Interscience, New York
Rosner,R., Tucker,W.H., Vaiana,G.S.: 1978, Astrophys.J. 220, 643
Scharmer,G.B.: 1984, Methods in radiative transfer, W.Kalkofen ed., Univ.Press, Cambridge, p.173
Scharmer,G.B., Carlsson,M.: 1985, J.Comput.Phys. 59, 56
Schmitz,F., Ulmschneider,P., Kalkofen,W.: 1985, Astron.Astrophys.148, 217
Spitzer,L.Jr.: 1962, Physics of Fully Ionized Gases, Interscience, New York
Stein,R.F.: 1966, in Stellar Evolution, R.F.Stein and A.G.W.Cameron eds., Plenum Press, New York, p.20
Stein,R.F., Leibacher,J.: 1974, Ann.Rev.Astron.Astrophys. 12, 407
Stein,R.F., Schwartz,R.A.: 1972, Astrophys.J. 177, 807
Stein,R.F., Schwartz,R.A.: 1973, Astrophys.J. 186, 1083
Tscharnuter,W.M., Winkler,K.-H.A.: 1979, Comp.Phys.Comm. 18, 171
Ulmschneider,P.: 1970, Astron.Astrophys. 4, 144
Ulmschneider,P.: 1979, Space Sci.Rev. 24, 71
Ulmschneider,P.: 1985, Proc. Workshop on Theoretical Problems in Solar Physics, Munich
Ulmschneider,P., Muchmore,D.: 1986, Astron.Astrophys., to be published
Ulmschneider,P., Nowak,T., Bohn,U.: 1977, Astron.Astrophys. 54, 61
Ulmschneider,P., Schmitz,F., Kalkofen,W., Bohn,H.U.: 1978, Astron. Astrophys. 70, 487
Vernazza,J.E., Avrett,E.H., Loeser,R.: 1981, Astrophys.J.Suppl. 45, 635
Von Neumann,J., Richtmyer,R.D.: 1950, J.Appl.Phys. 21, 232
Winkler,K.-H.A., Norman,M.L., Newman,M.J.: 1984, Physica 12D, 408
Wolf,B.E.: 1983, Astron.Astrophys. 127, 93
Wolf,B.E.: 1985a, Astron.Astrophys. 145, 278
Wolf,B.E.: 1985b, Ph.D. thesis, Univ. of Heidelberg
Wolf,B.E., Schmitz,F., Ulmschneider,P.: 1981, Astron.Astrophys. 97, 101
Wood,P.R.: 1979, Astrophys.J. 227, 220
Wu,S.T., Kan,L.C., Nakagawa,Y., Tandberg-Hanssen,E.: 1981, Solar Phys. 70, 137